crystals

MDPI

Article

Absolute Luminescence Efficiency of Europium-Doped Calcium Fluoride (CaF_2:Eu) Single Crystals under X-ray Excitation

Christos Michail [1,*], Nektarios Kalyvas [1], Athanasios Bakas [2], Konstantinos Ninos [2], Ioannis Sianoudis [2], George Fountos [1], Ioannis Kandarakis [1], George Panayiotakis [3] and Ioannis Valais [1]

1 Department of Biomedical Engineering, Radiation Physics, Materials Technology and Biomedical Imaging Laboratory, University of West Attica, Ag. Spyridonos, 12210 Athens, Greece; nkalyvas@uniwa.gr (N.K.); gfoun@uniwa.gr (G.F.); kandarakis@uniwa.gr (I.K.); valais@uniwa.gr (I.V.)
2 Department of Biomedical Sciences, University of West Attica, Ag. Spyridonos, 12210 Athens, Greece; abakas@uniwa.gr (A.B.); kninos@uniwa.gr (K.N.); jansian@uniwa.gr (I.S.)
3 Department of Medical Physics, Faculty of Medicine, University of Patras, 265 00 Patras, Greece; panayiot@upatras.gr
* Correspondence: michail@upatras.gr; Tel.: +30-210-5385-387

Received: 14 March 2019; Accepted: 28 April 2019; Published: 1 May 2019

Abstract: The absolute luminescence efficiency (AE) of a calcium fluoride (CaF_2:Eu) single crystal doped with europium was studied using X-ray energies met in general radiography. A CaF_2:Eu single crystal with dimensions of $10 \times 10 \times 10$ mm^3 was irradiated by X-rays. The emission light photon intensity of the CaF_2:Eu sample was evaluated by measuring AE within the X-ray range from 50 to 130 kV. The results of this work were compared with data obtained under similar conditions for the commercially employed medical imaging modalities, $Bi_4Ge_3O_{12}$ and Lu_2SiO_5:Ce single crystals. The compatibility of the light emitted by the CaF_2:Eu crystal, with the sensitivity of optical sensors, was also examined. The AE of the $10 \times 10 \times 10$ mm^3 CaF_2:Eu crystal peaked in the range from 70 to 90 kV (22.22 efficiency units; E.U). The light emitted from CaF_2:Eu is compatible with photocathodes, charge coupled devices (CCD), and silicon photomultipliers, which are used as radiation sensors in medical imaging systems. Considering the AE results in the examined energies, as well as the spectral compatibility with various photodetectors, a CaF_2:Eu single crystal could be considered for radiographic applications, including the detection of charged particles and soft gamma rays.

Keywords: inorganic scintillators; single crystals; radiation detectors; CaF_2:Eu

1. Introduction

The use of single crystals as radiation converters is very common in imaging or counting applications, especially when coupled with optical sensors such as photomultipliers, which are frequently employed in radiation detectors [1,2]. Additionally, they are widely used in particle physics, homeland security, and in numerous disciplines of medical imaging, such as X-ray computed and positron emission tomography (CT and PET, respectively), radiotherapy, radiography, and mammography [3–16].

The state-of-the-art electronics that are used in today's imaging systems require scintillators with exceptional properties, which are tailored for every application [1,17–19]. This is also a prerequisite for medical imaging, where the need for exceptional quality of the diagnostic images as well as the lowest possible radiation exposure of patients as directed by the ALARA principle (as low as reasonably achievable) is a priority [20]. In this scope, medical imaging detectors should incorporate

scintillators with optimized characteristics in terms of efficiency and imaging performance. An example is the time-of-flight (TOF) technique in PET scanners, requiring inorganic scintillators with primarily extremely short decay time, high density, and light yield (LY) [2,21]. Similar concerns arise in other fast applications such as CT, in which afterglow can cause blur in the final image [7].

During the last century, from the discovery of the very first scintillating materials, up to our era, various research groups have tried to improve and tailor the properties of scintillating materials for particular medical imaging applications [22–25]. For example, in positron emission tomography, single crystals have been used in order to detect high-energy coincident photons, which are produced after the emission of positrons from radioisotopes [26,27]. The use of scintillators with different properties has been extensively researched and explored by the scientific community, and currently, a number of single crystal materials have been adopted to be used in commercial PET scanners, such as lutetium oxyorthosilicate (LSO), bismuth germinate oxide (BGO), yttrium orthoaluminate perovskite (YAP), gadolinium oxyorthosilicate (GSO), among others [14,23,26,28–30]. LSO has been used as detector material, for example in the Biograph™6 PET/CT scanner (Siemens Medical Solutions), whereas BGO was used in the ECAT EXACT HR+ (Siemens Medical Solutions, Erlangen, Germany) and Discovery ST PET/CT (General Electric, Chicago, Illinois, US) PET scanners [31,32].

Europium-activated calcium fluoride (CaF_2:Eu) scintillators have already been incorporated in many different applications such as spectroscopy, charged particle detection, double beta decay investigation, the search for dark matter, low-energy radiation detectors, time-of-flight (TOF) applications, mobile Compton cameras, solar cell application, as well as homeland security [33–40]. Besides, due to its long decay constant, it was used in phoswich detectors [38,39,41,42]. Furthermore, CaF has been used as an efficient dosimeter material, due to the low atomic numbers of calcium (Z = 20) and fluorine (Z = 9), along with its effective atomic number (Z = 16.5), which is close to that of soft tissues.

Up until now, CaF has been used in a limited number of biomedical applications [22–25,43–52]. For example, CaF_2 has been applied in conjunction with SiPMs in gamma spectrometry, and due to its biocompatibility and the stability of the material, it has proven to be significant for fluorescent labeling in biological applications. Furthermore, the very good transparency in a wide wavelength range, the low refractive index, and the low phonon energy, make CaF_2 suitable to host luminescent ions, and thus a good choice for multimodal imaging [22,43,52–60].

CaF_2:Eu has been used and studied for decades, in single crystal and nanocrystal forms [43,52–60]. This material is cheap and can be prepared easily in large quantities. Europium-activated calcium fluoride is easily machined; it is also non-hygroscopic, inert, and insoluble (solubility 0.0017 g/100 g H_2O). The properties of this material are also compatible for particle and low-energy sensors, which are well suited to use within vacuums since it has very low-vapor pressure point. Furthermore, it is robust to thermal and mechanical shock, with a high melting point (1418 °C). It has low inherent background radiation, but due to the density value of 3.18 g/cm^3 and the low Z, the light yield is also relatively moderate (19,000 photons/MeV) and the output of the emitted light is approaching 60% of sodium iodide (Nal) doped with thallium. Thus, this material is not adequate for high-energy experiments. CaF_2:Eu has sharp maximum emission at around 435 nm and it can be used with titanium dioxide (TiO_2) as an efficient reflector, but has also partially overlapping absorption and emission around 400 nm. The index of refraction is 1.443, which is very close to that of most photomultiplier's glasses and silicon P-I-N photodiodes with shallow junctions. The band gap energy is large (12 eV), and the decay time is around 940 ns. The energy resolution is excellent (5.7–6.07% at 662 keV), taking into consideration the atomic value of this material [34–36,39,61–75].

In this study, the efficiency of a 10 × 10 × 10 mm CaF_2:Eu single crystal was measured in order to examine the performance of this material as a possible candidate for medical imaging applications against the established single crystals, taking into consideration distinct advantages, such as: (i) the light photons emitted by CaF_2 are approaching 60% of that of Nal:Tl, and (ii) contrary to LSO, it has no afterglow [24]. The light energy flux for exposure rates within a range of 80 kVps, covering X-ray

radiography examinations, was measured. Additionally, the light emitted by CaF_2:Eu was recorded and correlated with various optical sensors that are used in radiation detectors. The results of this study were compared with previously published results for Lu_2SiO_5:Ce and $Bi_4Ge_3O_{12}$ single crystals that are frequently used in commercial imaging systems. Finally, the stopping power of the crystals, described via the energy absorption efficiency (EAE), was calculated and compared to previously published data.

2. Materials and Methods

A CaF_2:Eu single crystal, with polished surfaces, was purchased from Advatech UK Limited [76]. The crystal had dimensions of $10 \times 10 \times 10$ mm. The crystal was irradiated by X-rays on a BMI Merate X-ray tube with inherent filtration equivalent to 2 mm of Al and added filtration of 20 mm of Al. The examined tube voltages span in a range of 80 kVps (50–130) [77].

2.1. Absolute and X-ray Luminescence Efficiency

In order to estimate the absolute and the X-ray luminescence efficiencies of the crystal sample, the light flux was measured using a light integration sphere (Oriel 70451), connected to a photomultiplier tube (PMT) (EMI 9798B). The signal of the PMT was fed to a Cary 401 vibrating reed electrometer and the exposure rate was measured with a calibrated dosimeter (RTI Piranha P100B) [78]. The measured emitted light from the single crystal, divided by the X-ray exposure, provided the absolute luminescence efficiency (AE), i.e., the energy flux of the emitted light $\dot{\Psi}_\lambda$, per unit of incident exposure rate $\dot{X}$:

$$\eta_A = \dot{\Psi}_\lambda / \dot{X} \tag{1}$$

The units of AE are given in $\mu W \times m^{-2} / (mR \times s^{-1})$ (efficiency units: E.U.).

Afterwards, the X-ray luminescence efficiency (*XLE*) was defined as the fraction of incident energy converted into emitted light; that is, $(\eta_\psi = \Psi_\Lambda / \Psi_0)$. XLE was determined by converting the X-ray exposure data that was used to calculate AE into X-ray energy flux (Ψ_0), as follows: $\Psi_0 = X\hat{\Psi}$ where $\hat{\Psi}$ is defined as the X-ray energy flux per exposure rate, estimated according to Equation (2):

$$\hat{\Psi} = \frac{\int \Psi_0(E) dE}{\int \Psi_0(E) \left[\frac{X}{\Psi_0(E)} \right] dE} = \frac{\int \Psi_0(E) dE}{\int \Psi_0(E) \left[\left(\frac{\mu_{en}(E)}{\rho} \right)_{air} \cdot \left(\frac{W_A}{e} \right)^{-1} \right] dE} \tag{2}$$

$(\mu_{en}/\rho)_{air}$ is the X-ray mass energy absorption coefficient of air, and (W_A/e) is the average energy per unit of charge required to produce an electron–ion pair in air, as obtained from tabulated data [79].

2.2. Spectral Matching

The percentage of the emitted light from a single crystal that can be detected by a sensor can be quantified using the factor of the spectral matching αs, which is given by Equation (3):

$$\alpha s = \int \phi\lambda(\lambda) SD(\lambda) d\lambda / \int \phi\lambda(\lambda) d\lambda \tag{3}$$

In Equation (3), $\phi\lambda(\lambda)$ is the emitted light, and $SD(\lambda)$ is the sensor's detection efficiency in particular wavelengths [78].

The emitted light was measured by a grating optical spectrometer (Ocean Optics Inc., HR2000). The spectral sensitivities of the optical detectors were obtained from tabulated data [80–84]. The effective efficiency (ηeff) was defined as the product of AE with the Spectral Matching Factor [84].

2.3. Energy Absorption Efficiency

The radiation detection properties of a scintillator can by quantified by the energy absorption efficiency (EAE) [85–87]. EAE expresses the energy locally deposited at the sites of primary photon interactions and is a useful parameter for characterizing the efficiency of planar scintillators. The energy absorption efficiency was calculated by Equation (4):

$$\langle \eta_{\varepsilon} \rangle_E = \frac{\int_0^{E_0} \Psi(E)\left(\frac{\mu_{tot,en}(E)}{\mu_{tot,t}(E)}\right)\eta q(E)dE}{\int_0^{E_0} \Psi(E)dE} \quad (4)$$

$\eta q(E)$ is the monoenergetic quantum efficiency. $\mu_{tot,t}(E)/\rho$ is the X-ray total mass attenuation coefficient of the scintillator, and $\mu_{tot,en}(E)/\rho$ is the total mass energy absorption coefficient of the scintillator, which includes all the mechanisms of energy deposition locally at the point of X-ray interaction within the crystal [79,88].

3. Results and Discussion

Figure 1 shows the AE results for the CaF_2:Eu single crystal in the examined energy range. The results were compared with published data, for LSO and BGO crystals of equal dimensions ($10 \times 10 \times 10$ mm^3) [28]. The AE of the CaF_2:Eu increased up to 80 kilovolts. From 80 to 130 kilovolts, the AE values progressively decreased. The maximum value at 80 kVp was 22.22 E.U. The $10 \times 10 \times 10$ mm^3 CaF_2:Eu crystal had increased AE compared to both LSO and BGO, across the examined kVp range [28]. However, for values higher than 90 kVp, the AE of the CaF_2:Eu crystal showed a tendency to decrease due to the lower density and Z value of CaF_2:Eu, which results also in low light yield (19000 photons/MeV) when interacting with higher energies [57]. In this energy range, the AE values of the $10 \times 10 \times 10$ mm^3 LSO crystal showed a constant increase (light yield ≥ 26,000 photons/MeV). BGO, due to the low light yield (8200 photons/MeV), showed lower AE values. Figure 1 also shows XLE results (right Y axis) for the $10 \times 10 \times 10$ mm^3 CaF_2:Eu and LSO crystals in the examined energy range. The BGO data were excluded, since their values were hardly visible in the graph. The X-ray luminescence efficiency of CaF_2:Eu constantly decreases within the radiographic energies, showing a maximum at 50 kVp. The XLE of LSO increases up to 70 kVp and remains almost constant thereafter. This behavior is influenced by the X-ray mass energy absorption coefficients of air $(\mu_{en}/\rho)_{air}$ in this energy range and the average energy per unit of charge that is required to produce an electronion pair in air (W_A/e); the latter is used upon the conversion of X-ray exposure data into X-ray energy flux, in order to determine the fraction of incident energy converted into emitted light.

The luminescence efficiency results indicate that the AE values of CaF_2 were higher than both the commercial employed LSO and BGO single crystals, across the examined energy range, thus supporting the main hypothesis of the current study regarding the possibility of application of CaF_2 in medical imaging applications. This finding is significant for medical imaging modalities lying in this energy range. For higher energies, CaF_2 efficiency shows a tendency to decrease, thus suggesting that it would not be efficient for nuclear medicine applications.

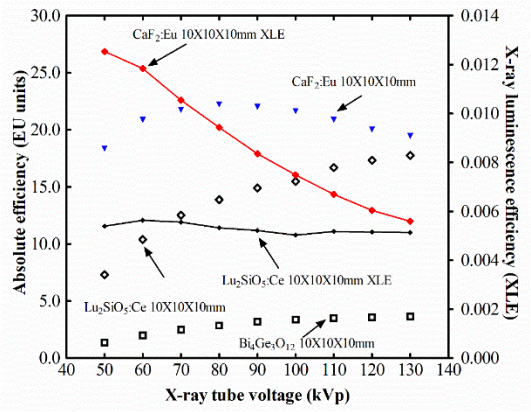

Figure 1. Absolute luminescence efficiency (AE) and X-ray luminescence efficiency (XLE) results for the $10 \times 10 \times 10$ mm^3 CaF_2:Eu crystals. Comparison of the AE results with published data for lutetium oxyorthosilicate (LSO) and bismuth germinate oxide (BGO).

Figure 2a–d show the normalized emitted optical spectrum of CaF_2:Eu crystal upon excitation with UV light. The spectral data are shown along with the sensitivity values of a variety of optical sensors. Figure 2a,b show mostly the spectral sensitivities of various PMTs and photocathodes used in nuclear medicine techniques. Figure 2c,d show the spectral sensitivities of various charge-coupled devices (CCD) and complementary metal–oxide semiconductors (CMOS) used in imaging modalities. The transition of the Eu ions with oxidation state of +2, in CaF_2, from the $4f^6 5d^1$ levels configuration to the $4f^7$ ground state configuration, result in a near ultraviolet, bluish emission maximum at 424 nm, with a full-width-at-half-maximum (FWHM) of about 29 nm, which is close to previously published values [89–91].

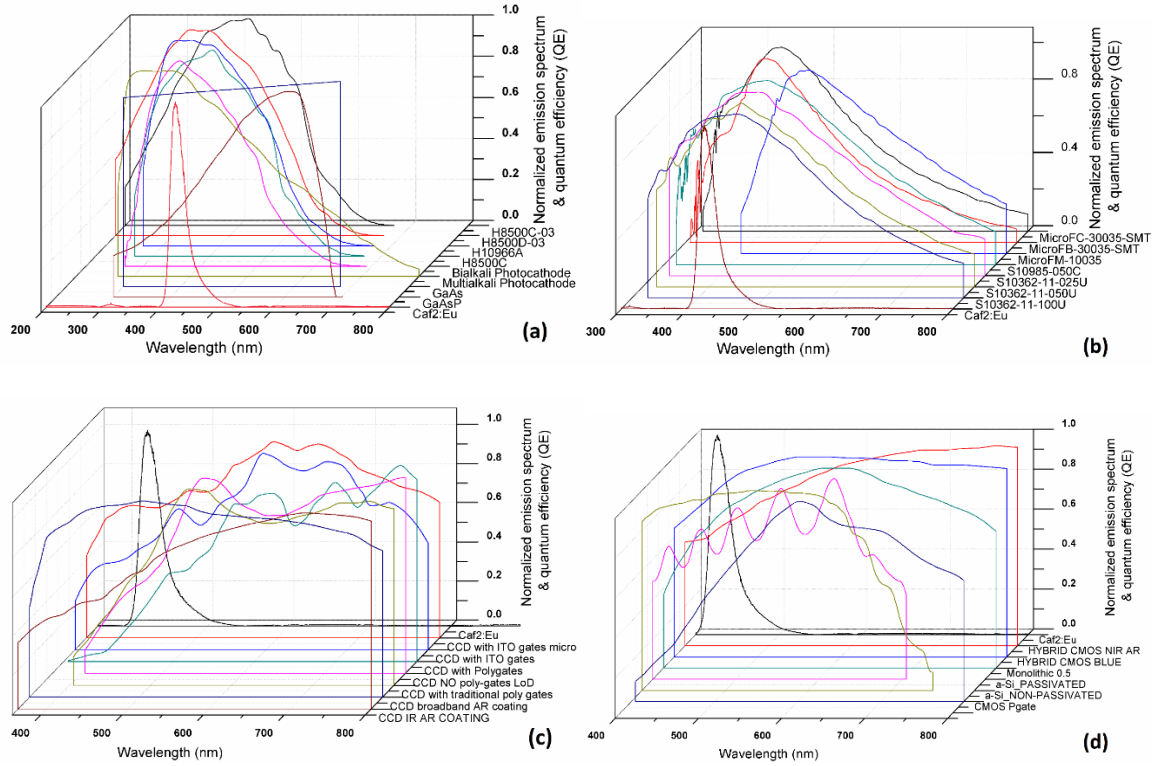

Figure 2. CaF_2:Eu single crystal emitted spectrum along with the sensitivity of: (**a**) and (**b**) photomultiplier tube (PMTs) and photocathodes, (**c**) charge-coupled devices (CCDs), (**d**) complementary metal–oxide semiconductor (CMOS) sensors, and amorphous hydrogenated silicon photodiodes.

The spectral matching factor data for CaF_2:Eu in conjunction with various optical sensors used in medical imaging detectors are shown in Table 1. CaF_2:Eu is compatible with Multi-Pixel Photon Counters (MPPC) silicon (Si) PMTs (SMF = 0.96 with Hamamatsu Si PM S10362-11-025U and S10362-11-100U, SMF = 0.95 with S10985 and S10362-11-050U). Furthermore CaF_2:Eu was compatible with the following photocathodes: the gallium arsenide GaAs (0.95) and the extended (E-S20) photocathodes (0.94). The same value was found for spectral matching when coupled with charge-coupled devices (0.94) and the Sensl's MicroFC-30035 (0.94) silicon PMT. The spectral matching value for a non-passivated amorphous hydrogenated silicon photodiode (a-Si:H), was 0.92, but only 0.63 with a passivated a-Si:H. It was also found to be compatible with Hamamatsu PS-PMTs, such as the H8500C-03 (0.91). When coupled with certain types of complementary metal–oxide semiconductors, the spectral matching value was found to be 0.79.

CaF_2:Eu also showed good compatibility with a monolithic (0.25 μm) (0.64) and high-resolution RadEye complementary metal–oxide semiconductor (0.68), and with a CCD with indium tin oxide gates with microlenses (0.68).

It was found to have moderate compatibility with Sensl's silicon photomultiplier MicroFM-10035 (0.61). CaF_2:Eu was found to be incompatible with a CCD having polygates (0.18) and a CMOS with photogate array (0.26).

Table 1. Spectral matching factor data.

Light Sensors	CaF_2:Eu	Light Sensors	CaF_2:Eu
CCD broadband AR coating	0.94	GaAsP phosphor photocathode	0.52
CCD infrared (IR) anti-reflection (AR) coating	0.54	Extended photocathode (E-S20)	0.94
CMOS hybrid with blue anti-reflection (AR) coating	0.60	Si PM MicroFC-30035-SMT	0.94
Hybrid CMOS blue	0.79	Si PM MicroFB-30035-SMT	0.92
CMOS (monolithic 0.25 μm)	0.64	Si PM MicroFM-10035	0.61
a-Si:H passivated	0.63	Si PM S10985-050C	0.95
a-Si:H_non-passivated	0.92	Si PM S10362-11-025U	0.96
CCD with indium tin oxide (ITO) gates with microlenses	0.68	Si PM S10362-11-050U	0.95
CCD with indium tin oxide (ITO) gates	0.51	Si PM S10362-11-100U	0.96
CCD with poly gates	0.18	Flat panel PS-PMT H8500C-03	0.91
CCD no poly gates LoD	0.34	Flat panel PS-PMT H8500D-03	0.78
CCD with traditional poly gates	0.34	Flat panel PS-PMT H10966A	0.79
CMOS (photogate array 0.5 μm)	0.26	Flat panel PS-PMT H8500C	0.86
CMOS RadEye HR	0.68	Bialkali Photocathode	0.78
GaAs Photocathode	0.95	Multialkali Photocathode	0.81

Figure 3 shows the luminescence efficiency of the $10 \times 10 \times 10$ mm^3 CaF_2:Eu crystal, degraded by the spectral matching values when coupled with various optical sensors. Following the results of Table 1, the highest effective efficiency value was attributed to CaF_2:Eu/Hamamatsu MPPC Si-PMT. The lowest values are shown when matched with certain CCD types with optimum sensitivity toward the red part of the light spectrum.

Figure 4 shows values for the EAE of the 10-mm thick CaF_2:Eu crystal along with a comparison with LSO and BGO crystals incorporated in commercial imaging units. The difference of all these values from unity is explained considering that EAE neglects mechanisms of interaction inside the crystal, such as scattered, characteristic, and bremsstrahlung radiation. The EAE values of CaF_2:Eu crystal (0.82 at 40 kV) were lower than both BGO (0.834 at 40 kV) and LSO (0.875 at 40 kV) due to the considerably higher density of these materials (7.13 and 7.4 g/cm^3, respectively) in respect to the 3.18 g/cm^3 of CaF_2:Eu. The difference between the absorption efficiency values of CaF_2, in respect to those of LSO and BGO, increases with the increase in X-ray energies. This result is in accordance with the luminescence efficiency behavior that is shown in Figure 1 for higher energies; thus, this material would not be efficient for nuclear medicine applications.

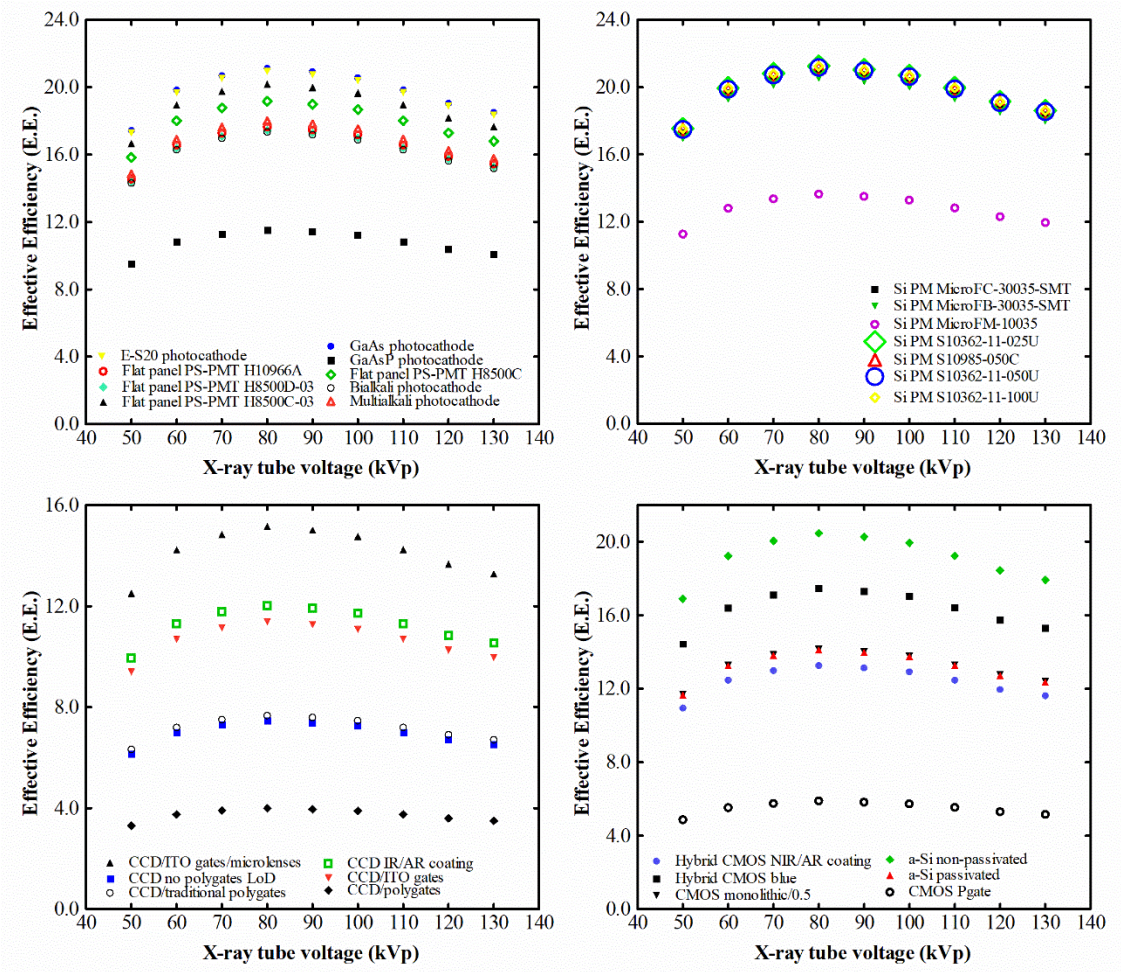

Figure 3. Effective efficiency of the CaF_2:Eu single crystal.

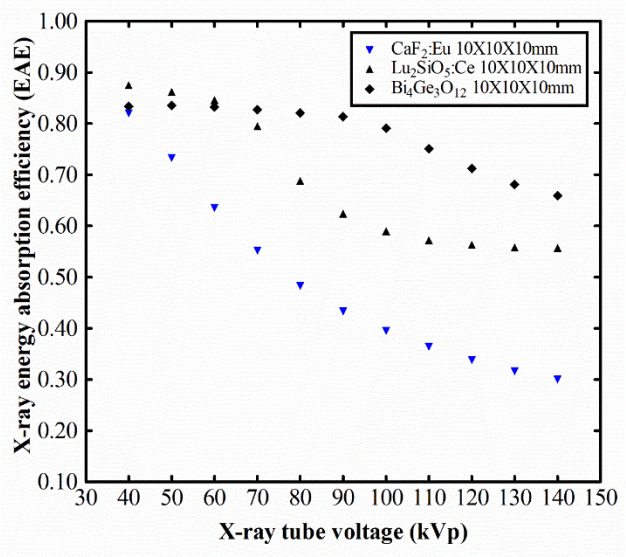

Figure 4. Energy absorption efficiency (EAE) of the CaF_2:Eu crystal along with data for LSO and BGO.

4. Conclusions

The absolute luminescence efficiency and the spectral matching of a CaF_2:Eu crystal were investigated in conditions usually met in general radiography. The results were compared with data of crystals with equal dimensions, which are frequently used in commercial imaging modalities,

such as LSO and BGO. The examined sample showed optimum efficiency at an X-ray tube voltage of 80 kV. The luminescence efficiency of the $10 \times 10 \times 10$ mm^3 CaF_2:Eu sample showed increased values compared to both LSO and BGO across the examined energy range. The light emitted from the CaF_2:Eu was found to be compatible with commercial photocathodes, charge-coupled devices (CCD), and SiMTs. CaF_2:Eu could be potentially used in radiographic applications due to the promising absolute efficiency values in the radiographic energy range, as well as the matching of the emitted light with commercial optical sensors, besides the detection of charged particles and soft gamma rays.

Author Contributions: Conceptualization, C.M. and I.G.; methodology, C.M., I.G., N.K., G.P and I.K.; software, I.S.; validation, N.K. and G.P.; formal analysis, C.M., N.K., G.P. and I.G.; investigation, C.M., N.K., G.P., K.N. and I.G.; resources, K.N. and A.B.; data curation, C.M., N.K., G.P. and I.G.; writing—original draft preparation, C.M.; writing—review and editing, I.K., G.P. and I.G.; visualization, C.M.; supervision, I.G.; project administration, C.M., K.N. and I.G.; funding acquisition, G.P. and K.N.

Funding: This research was funded by the Institutional Open Access Program (IOAP) of the University of Patras and the University of West Attica.

Conflicts of Interest: The authors declare no conflict of interest.

References

1. Salomoni, M.; Pots, R.; Auffray, E.; Lecoq, P. Enhancing Light Extraction of Inorganic Scintillators Using Photonic Crystals. *Crystals* **2018**, *8*, 78. [CrossRef]
2. Maddalena, F.; Tjahjana, L.; Xie, A.; Arramel, A.; Zeng, S.; Wang, H.; Coquet, P.; Drozdowski, W.; Dujardin, C.; Dang, C.; et al. Inorganic, Organic, and Perovskite Halides with Nanotechnology for High–Light Yield X- and γ-ray Scintillators. *Crystals* **2019**, *9*, 88. [CrossRef]
3. Drozdowski, W.; Brylew, K.; Chruścińska, A.; Kamada, K.; Yanagida, T.; Yoshikawa, A. Scintillation yield enhancement in LuAG:Pr crystals following thermal annealing. *Opt. Mater.* **2012**, *34*, 1975–1978. [CrossRef]
4. Michail, C.; Karpetas, G.; Kalyvas, N.; Valais, I.; Kandarakis, I.; Agavanakis, K.; Panayiotakis, G.; Fountos, G. Information Capacity of Positron Emission Tomography Scanners. *Crystals* **2018**, *8*, 459. [CrossRef]
5. Mares, J.; Nikl, M.; Beitlerova, A.; Horodysky, P.; Blazek, K.; Bartos, K.; D'Ambrosio, C. Scintillation Properties of Ce^{3+}-and Pr^{3+}-Doped LuAG, YAG and Mixed $Lu_xY_{1-x}AG$ Garnet Crystals. *IEEE Trans. Nucl. Sci.* **2012**, *59*, 2120–2125. [CrossRef]
6. Mares, J.; Beitlerova, A.; Nikl, M.; Vedda, A.; D'Ambrosio, C.; Blazek, K.; Nejezchleb, K. Time development of scintillating response in Ce- or Pr-doped crystals. *Phys. Stat. Sol. C* **2007**, *4*, 996–999. [CrossRef]
7. Hu, Z.; Chen, X.; Chen, H.; Shi, Y.; Liu, X.; Xie, T.; Kou, H.; Pan, Y.; Mihokova, E.; Nikl, M.; et al. Suppression of the slow scintillation component of $Pr:Lu_3Al_50_{12}$ transparent ceramics by increasing Pr concentration. *J. Lumin.* **2019**, *210*, 14–20. [CrossRef]
8. Nikl, M.; Pejchal, J.; Mihokova, E.; Mares, J.; Ogino, H.; Yoshikawa, A.; Fukuda, T.; Vedda, A.; D'Ambrosio, C. Antisite defect-free $Lu_3(Ga_xAl_{1-x})_5O_{12}$:$PrLu_3(Ga_xAl_{1-x})_5O_{12}$:Pr scintillator. *Appl. Phys. Lett.* **2006**, *88*, 141916. [CrossRef]
9. Kamada, K.; Tsutsumi, K.; Usuki, Y.; Ogino, H.; Yanagida, T.; Yoshikawa, A. Crystal Growth and Scintillation Properties of 2-Inch-Diameter $Pr:Lu_3Al_5O_{12}$ (Pr:LuAG) Single Crystal. *IEEE Trans. Nucl. Sci.* **2008**, *55*, 1488–1491. [CrossRef]
10. Yoshikawa, A.; Yanagida, T.; Kamada, K.; Yokota, Y.; Pejchal, J.; Usuki, Y.; Yamamoto, S.; Miyake, M.; Kumagai, K.; Yamaji, A.; et al. Positron emission mammography using Pr:LuAG scintillator—Fusion of optical material study and systems engineering. *Opt. Mater.* **2010**, *32*, 1294–1297. [CrossRef]
11. Ogino, H.; Yoshikawa, A.; Nikl, M.; Krasnikov, A.; Kamada, K.; Fukuda, T. Growth and scintillation properties of Pr-doped Lu. *J. Cryst. Growth* **2006**, *287*, 335–338. [CrossRef]
12. Yanagida, T.; Yoshikawa, A.; Yokota, Y.; Kamada, K.; Usuki, Y.; Yamamoto, S.; Miyake, M.; Baba, M.; Kumagai, K.; Sasaki, K.; et al. Development of Pr:LuAG Scintillator Array and Assembly for Positron Emission Mammography. *IEEE Trans. Nucl. Sci.* **2010**, *57*, 1492–1495. [CrossRef]
13. Valais, I.; Kandarakis, I.; Nikolopoulos, D.; Michail, C.; David, S.; Loudos, G.; Cavouras, D.; Panayiotakis, G. Luminescence properties of $(Lu,Y)_2SiO_5$:Ce and Gd_2SiO_5:Ce single crystal scintillators under X-ray excitation for use in medical imaging systems. *IEEE Trans. Nucl. Sci.* **2007**, *54*, 11–18. [CrossRef]

14. Valais, I.; Michail, C.; David, S.; Liaparinos, P.; Fountos, G.; Paschalis, T.; Kandarakis, I.; Panayiotakis, G. Comparative Investigation of Ce^{3+} doped Scintillators in a wide Range of Photon Energies covering X-ray CT, Nuclear Medicine and Megavoltage Radiation Therapy Portal Imaging applications. *IEEE Trans. Nucl. Sci.* **2010**, *57*, 3–7. [CrossRef]
15. Michail, C.; David, S.; Liaparinos, P.; Valais, I.; Nikolopoulos, D.; Kalivas, N.; Toutountzis, A.; Cavouras, D.; Kandarakis, I.; Panayiotakis, G. Evaluation of the imaging performance of LSO powder scintillator for use in X-ray mammography. *Nucl. Instrum. Meth. Phys. Res. A* **2007**, *580*, 558–561. [CrossRef]
16. Michail, C.; Valais, I.; Martini, N.; Koukou, V.; Kalyvas, N.; Bakas, A.; Kandarakis, I.; Fountos, G. Determination of the Detective Quantum Efficiency (DQE) of CMOS/CsI Imaging Detectors following the novel IEC 62220-1-1:2015 International Standard. *Radiat. Meas.* **2016**, *94*, 8–17. [CrossRef]
17. Kato, T.; Kataoka, J.; Nakamori, T.; Miura, T.; Matsuda, H.; Sato, K.; Ishikawa, Y.; Kawabata, N.; Ikeda, H.; Sato, G.; et al. Development of a large-area monolithic 4X4 MPPC array for a future PET scanner employing pixelized Ce:LYSO and Pr:LuAG crystals. *Nucl. Instrum. Meth. Phys. Res. A* **2011**, *638*, 83–91. [CrossRef]
18. Hu, C.; Li, J.; Yang, F.; Jiang, B.; Zhang, L.; Zhu, R. LuAG ceramic scintillators for future HEP experiments. *Nucl. Instrum. Meth. Phys. Res. A* **2019**. [CrossRef]
19. Kastengren, A. Thermal behavior of single-crystal scintillators for high-speed X-ray imaging. *J. Synchrotron Rad.* **2019**, *26*, 205–214. [CrossRef]
20. Grammaticos, P.; Fountos, G. The physician should benefit, not harm the patient. *Hell. J. Nucl. Med.* **2006**, *9*, 82–84.
21. Gundacker, S.; Martinez Turtos, R.; Auffray, E.; Paganoni, M.; Lecoq, P. High-frequency SiPM readout advances measured coincidence time resolution limits in TOF-PET. *Phys. Med. Biol.* **2019**, *64*, 055012. [CrossRef] [PubMed]
22. Grodzicka, M.; Moszynski, M.; Szczesniak, T. Silicon Photomultipliers in Detectors for Nuclear Medicine. In *Radiation Detectors for Medical Imaging Devices, Circuits, and Systems*; Iniewski, K., Iwanczyk, J., Eds.; CRC Press: Boca Raton, FL, USA, 2016; pp. 119–148.
23. Gupta, T. *Radiation, Ionization, and Detection in Nuclear Medicine*; Springer: Heidelberg, Germany, 2013.
24. Preston, K., Jr.; Taylor, K.; Johnson, S.; Ayers, W. *Medical Imaging Techniques, a Comparison*; Plenum Press: New York, NY, USA, 1979.
25. Lecoq, P.; Korzhik, M.; Alexander Gektin, A. *Inorganic Scintillators for Detector Systems. Physical Principles and Crystal Engineering*; Springer: Cham, Switzerland, 2017.
26. Michail, C.; Karpetas, G.; Fountos, G.; Kalyvas, N.; Valais, I.; Fountzoula, C.; Zanglis, A.; Kandarakis, I.; Panayiotakis, G. A novel method for the Optimization of Positron Emission Tomography Scanners Imaging Performance. *Hell. J. Nucl. Med.* **2016**, *19*, 231–240. [PubMed]
27. Vaquero, J.; Kinahan, P. Positron Emission Tomography: Current Challenges and Opportunities for Technological Advances in Clinical and Preclinical Imaging Systems. *Annu. Rev. Biomed. Eng.* **2015**, *17*, 385–414. [CrossRef] [PubMed]
28. Valais, I.; Michail, C.; David, S.; Nomicos, C.; Panayiotakis, G.; Kandarakis, I. A Comparative Study of the Luminescence Properties of LYSO:Ce, LSO:Ce, GSO:Ce and BGO Single Crystal Scintillators for Use in Medical X-ray Imaging. *Phys. Med.* **2008**, *24*, 122–125. [CrossRef] [PubMed]
29. Van Eijk, C. Inorganic scintillators in medical imaging. *Phys. Med. Biol.* **2002**, *47*, R85–R106. [CrossRef] [PubMed]
30. Humm, J.; Rosenfeld, A.; Guerra, A. From PET detectors to PET scanners. *Eur. J. Nucl. Med. Mol. Imaging* **2003**, *30*, 1574–1597. [CrossRef]
31. Trébossen, R.; Comtat, C.; Brulon, V.; Bailly, P.; Meyer, M. Comparison of two commercial whole body PET systems based on LSO and BGO crystals respectively for brain imaging. *Med. Phys.* **2009**, *36*, 1399–1409.
32. Karpetas, G.; Michail, C.; Fountos, G.; Kalyvas, N.; Valais, I.; Kandarakis, I.; Panayiotakis, G. Detective Quantum Efficiency (DQE) in PET Scanners: A Simulation Study. *Appl. Radiat. Isot.* **2017**, *125*, 154–162. [CrossRef]
33. Hong, B.; Kawano, K. Syntheses of Eu-Activated Alkaline Earth Fluoride MF_2 (M=Ca, Sr) Nanoparticles. *Jpn. J. Appl. Phys.* **2007**, *46*, 6319–6323. [CrossRef]
34. Holl, I.; Lorenz, E.; Mageras, G. A Measurement of the Light Yield of Common Inorganic Scintillators. *IEEE Trans. Nucl. Sci.* **1988**, *35*, 105–109. [CrossRef]
35. Knoll, G. *Radiation Detection and Measurement*; John Wiley and Sons: Hoboken, NJ, USA, 2000.

36. Shimizu, Y.; Minowa, M.; Suganuma, W.; Inoue, Y. Dark matter search experiment with CaF_2(Eu) scintillator at Kamioka Observatory. *Phys. Lett. B* **2006**, *633*, 195–200. [CrossRef]
37. Chen, M. Double beta decay: Scintillators. *J. Phys. Conf. Ser.* **2008**, *136*, 022035. [CrossRef]
38. Ely, J.; Aalseth, C.; McIntyre, J. Novel beta-gamma coincidence measurements using phoswich detectors. *J. Radioanal. Nucl. Chem.* **2005**, *263*, 245–250. [CrossRef]
39. Plettner, C.; Pausch, G.; Scherwinski, F.; Herbach, C.; Lentering, R.; Kong, Y.; Römer, K.; Grodzicka, M.; Szcześniak, T.; Iwanowska, J.; et al. CaF_2(Eu): An "old" scintillator revisited. *J. Inst.* **2013**, *8*, P06010. [CrossRef]
40. Bernabei, R.; Belli, P.; Montecchia, F.; Incicchitti, A.; Nicolantonio, W.; Prosperi, D.; Bacci, C.; Dai, C.; Ding, L.; Kuang, H.; et al. Improved limits on WIMP-^{19}F elastic scattering and first limit on the 2EC2ν ^{40}Ca decay by using a low radioactive CaF_2(Eu) scintillator. *Astropart. Phys.* **1997**, *7*, 73–76. [CrossRef]
41. Sunta, C. A review of thermoluminescence of calcium fluoride, calcium sulphate and calcium carbonate. *Radiat. Prot. Dosim.* **1984**, *8*, 25–44. [CrossRef]
42. Takada, M.; Shibata, T.; Uwamino, Y.; Nakamura, T. A performance study on a phoswich detector consisting of an inner NE213 scintillator and an outer CaF_2(Eu) crystal wall. *Nucl. Instrum. Meth. A* **1996**, *379*, 293. [CrossRef]
43. Song, L.; Gao, J.; Song, R. Synthesis and luminescent properties of oleic acid (OA)-modified CaF_2:Eu nanocrystals. *J. Lumin.* **2010**, *130*, 1179–1182. [CrossRef]
44. Wang, Y.; Zhao, Y.; White, D.; Finch, A.; Townsend, P. Factors controlling the thermoluminescence spectra of rare earth doped calcium fluoride. *J. Lumin.* **2017**, *184*, 55–63. [CrossRef]
45. Dubey, V.; Kaur, J.; Agrawal, S. Effect of europium concentration on photoluminescence and thermoluminescence behavior of Y_2O_3:Eu^{3+} Phosphor. *Res. Chem. Intermed.* **2015**, *41*, 4727–4739. [CrossRef]
46. Reddy, B.; Colon, T. White light emission characteristics of europium doped fluoride crystals. *Proc. SPIE* **2013**, *8621*, 86210.
47. Straßer, M.; Schrauth, J.; Dembski, S.; Haddad, D.; Ahrens, B.; Schweizer, S.; Christ, B.; Cubukova, A.; Metzger, M.; Walles, H.; et al. Calcium fluoride based multifunctional nanoparticles for multimodal imaging. *Beilstein J. Nanotechnol.* **2017**, *8*, 1484–1493. [CrossRef] [PubMed]
48. Nakhaei, O.; Shahtahmassebi, N. Study structural and up-conversion luminescence properties of polyvinyl alcohol/CaF:erbium nanofibers for potential medical applications. *Nanomed. J.* **2015**, *2*, 160–166.
49. Zhi, G.; Song, J.; Mei, B.; Zhou, W. Synthesis and characterization of Er^{3+} doped CaF_2 nanoparticles. *J. Alloys Compd.* **2011**, *509*, 9133–9137. [CrossRef]
50. Dong, N.-N.; Pedroni, M.; Piccinelli, F.; Conti, G.; Sbarbati, A.; Ramírez-Hernández, J.; Maestro, L.; Iglesias-de la Cruz, M.; Sanz-Rodriguez, F.; Juarranz, A.; et al. NIR-to-NIR Two-Photon Excited CaF_2:Tm^{3+},Yb^{3+} Nanoparticles: Multifunctional Nanoprobes for Highly Penetrating Fluorescence Bio-Imaging. *ACS Nano* **2011**, *5*, 8665–8671. [CrossRef] [PubMed]
51. Wang, G.; Peng, Q.; Li, Y. Upconversion Luminescence of Monodisperse CaF_2:Yb^{3+}/Er^{3+} Nanocrystals. *J. Am. Chem. Soc.* **2009**, *131*, 14200–14201. [CrossRef]
52. Bensalaha, A.; Mortiera, M.; Patriarcheb, G.; Gredinc, P.; Viviena, D. Synthesis and optical characterizations of undoped and rare-earth-doped CaF_2 nanoparticles. *J. Solid State Chem.* **2006**, *179*, 2636–2644. [CrossRef]
53. Wang, F.; Fan, X.; Pi, D.; Wang, M. Synthesis and luminescence behavior of Eu^{3+}-doped CaF_2 nanoparticles. *Solid State Commun.* **2005**, *133*, 775–779. [CrossRef]
54. Wang, J.; Miao, W.; Li, Y.; Yao, H.; Li, Z. Water-soluble Ln^{3+}-doped calcium fluoride nanocrystals: Controlled synthesis and luminescence properties. *Mater. Lett.* **2009**, *63*, 1794–1796. [CrossRef]
55. Salah, N.; Alharbi, N.; Habib, S.; Lochab, S. Luminescence Properties of CaF_2 Nanostructure Activated by Different Elements. *J. Nanomater.* **2015**, *2015*, 136402. [CrossRef]
56. Fan, T.; Lü, J.; Huang, Y.; Li, G. Monodispersing Eu^{3+} and Li^+ codoped CaF_2 nanoparticles for efficient luminescence. *Micro. Nano Lett.* **2018**, *13*, 393–396. [CrossRef]
57. Lina, L.; Leitnera, D.; Benattia, C.; Perdikakis, G.; Krausea, S.; Rencsoka, R.; Nasha, S.; Wittmer, W. Investigation of ion induced damage in KBr, YAG:Ce, CaF_2:Eu and CsI:Tl irradiated by various-energy protons. *J. Inst.* **2015**, *10*, P03024. [CrossRef]
58. Dujardin, C.; Auffray, E.; Bourret-Courchesne, E.; Dorenbos, P.; Lecoq, P.; Nikl, M.; Vasil'ev, A.; Yoshikawa, A.; Zh, R. Needs, Trends, and Advances in Inorganic Scintillators. *IEEE Trans. Nucl. Sci.* **2018**, *65*, 1977–1997. [CrossRef]

59. Yanagida, T. Inorganic scintillating materials and scintillation detectors. *Proc. Jpn. Acad. Ser. B* **2018**, *94*, 75–97. [CrossRef] [PubMed]
60. Cortelletti, P.; Pedroni, M.; Boschi, F.; Pin, S.; Ghigna, P.; Canton, P.; Vetrone, F.; Speghini, A. Luminescence of Eu^{3+} Activated CaF_2 and SrF_2 Nanoparticles: Effect of the Particle Size and Codoping with Alkaline Ions. *Cryst. Growth Des.* **2018**, *18*, 686–694. [CrossRef]
61. Sasidharan, S.; Jayasree, A.; Fazal, S.; Koyakutty, M.; Nair, S.; Menon, D. Ambient temperature synthesis of citrate stabilized and biofunctionalized, fluorescent calcium fluoride nanocrystals for targeted labeling of cancer cells. *Biomater. Sci.* **2013**, *1*, 294–305. [CrossRef]
62. Maushake, P. Calcium Fluoride Crystals. *Opt. Photonik* **2008**, *2*, 46–47. [CrossRef]
63. Belli, P.; Bernabei, R.; Dai, C.; Grianti, F.; He, H.; Incicchitti, A.; Kuang, H.; Ma, J.; Montecchia, F.; Ignesti, G.; et al. New limits on spin-dependent coupled WIMPs and on 2β processes in ^{40}Ca and ^{46}Ca by using low radioactive CaF_2(Eu) crystal scintillators. *Nucl. Phys. B* **1999**, *563*, 97–106. [CrossRef]
64. Heath, R.; Hofstadter, R.; Hughes, E. Inorganic scintillators: A review of techniques and applications. *Nucl. Instr. Meth.* **1979**, *162*, 431–476. [CrossRef]
65. Menefee, J.; Sweinehart, C.; O'Dell, E. Calcium fluoride as an X-ray and charged particle detector. *IEEE Trans. Nucl. Sci.* **1966**, *13*, 720–724. [CrossRef]
66. Shcheulin, A.; Semenova, T.; Koryakina, L.; Petrova, M.; Angervaks, A.; Ryskin, A. Additive coloring rate and intensity for pure and doped fluorite crystals. *Opt. Spectroscop.* **2011**, *110*, 617–623. [CrossRef]
67. Nakamura, F.; Kato, T.; Okada, G.; Kawaguchi, N.; Fukuda, K.; Yanagida, T. Scintillation and dosimeter properties of CaF_2 translucent ceramic produced by SPS. *J. Eur. Ceram. Soc.* **2017**, *37*, 1707–1711. [CrossRef]
68. Heaton, R.; Lin, C. Electronic energy-band structure of the calcium fluride crystal. *Phys. Rev. B* **1980**, *22*, 3629. [CrossRef]
69. Mikhailik, V.; Kraus, H.; Imber, J.; Wahl, D. Scintillation properties of pure CaF_2. *Nucl. Instrum. Meth. Phys. Res. A* **2006**, *566*, 522–525. [CrossRef]
70. Aliaga-Kelly, D.; Nicoll, D. Recent developments in scintillation detectors. *Nucl. Instrum. Meth.* **1966**, *43*, 110–115. [CrossRef]
71. Taulbeel, T.; Rooney, B.; Mengesha, W.; Valentine, J. The Measured Electron Response Nonproportionality of CaF_2, BGO, LSO, and GSO. *IEEE Nucl. Sci. Symp. Conf. Rec.* **1996**, *1*, 326–330.
72. Wang, J.; Yang, J.; Hu, T.; Chen, X.; Lang, J.; Wu, X.; Zhang, J.; Zhao, H.; Yang, J.; Cui, Q. Structural Phase Transition and Compressibility of CaF_2 Nanocrystals under High Pressure. *Crystals* **2018**, *8*, 199. [CrossRef]
73. Daví, F. Decay Time Estimates by a Continuum Model for Inorganic Scintillators. *Crystals* **2019**, *9*, 41. [CrossRef]
74. Hu, T.; Cui, X.; Wang, J.; Zhong, X.; Chen, Y.; Zhang, J.; Li, X.; Yang, J.; Gao, C. The Electrical Properties of Tb-Doped CaF_2 Nanoparticles under High Pressure. *Crystals* **2018**, *8*, 98. [CrossRef]
75. Di Tommaso, D.; Prakash, M.; Lemaire, T.; Lewerenz, M.; De Leeuw, N.; Naili, S. Molecular Dynamics Simulations of Hydroxyapatite Nanopores in Contact with Electrolyte Solutions: The Effect of Nanoconfinement and Solvated Ions on the Surface Reactivity and the Structural, Dynamical, and Vibrational Properties of Water. *Crystals* **2017**, *7*, 57. [CrossRef]
76. Advatech UK. CaF_2(Eu)—Calcium Fluoride (Eu). Available online: https://www.advatech-uk.co.uk/caf2_eu.html (accessed on 25 January 2019).
77. Michail, C.; Valais, I.; Fountos, G.; Bakas, A.; Fountzoula, C.; Kalyvas, N.; Karabotsos, A.; Sianoudis, I.; Kandarakis, I. Luminescence Efficiency of Calcium Tungstate ($CaWO_4$) under X-ray radiation: Comparison with Gd_2O_2S:Tb. *Measurement* **2018**, *120*, 213–220. [CrossRef]
78. Michail, C.; Valais, I.; Seferis, I.; Kalyvas, N.; David, S.; Fountos, G.; Kandarakis, I. Measurement of the Luminescence properties of Gd_2O_2S:Pr,Ce,F Powder Scintillators under X-ray radiation. *Radiat. Meas.* **2014**, *70*, 59–64. [CrossRef]
79. Hubbell, J.; Seltzer, S. *Tables of X-ray Mass Attenuation Coefficients and Mass Energy Absorption Coefficients 1 to 20 MeV for Elements Z = 1 to 92 and 48 Additional Substances of Dosimetric Interest*; NISTIR 5632; US Department of Commerce: Washington, DC, USA, 1995.
80. Hamamatsu Photonics, MPPC (Multi-Pixel Photon Counters). Available online: http://www.hamamatsu.com/us/en/product/category/3100/4004/4113/index.html# (accessed on 3 December 2018).
81. SensL. Silicon Photomultipliers. Available online: http://sensl.com/products/silicon-photomultipliers/ (accessed on 3 December 2018).

82. Rowlands, J.A.; Yorkston, J. Flat Panel Detectors for Digital Radiography. In *Handbook of Medical Imaging Physics and Psychophysics*; Beutel, J., Kundel, H., Van Metter, R., Eds.; SPIE: Bellingham, WA, USA, 2000; Volume 1, pp. 223–328. ISBN 9780819477729.
83. Magnan, P. Detection of visible photons in CCD and CMOS: A comparative view. *Nucl. Instrum. Meth. Phys. Res. A* **2003**, *504*, 199–212. [CrossRef]
84. Michail, C.; Kalyvas, N.; Valais, I.; David, S.; Seferis, I.; Toutountzis, A.; Karabotsos, A.; Liaparinos, P.; Fountos, G.; Kandarakis, I. On the response of $GdAlO_3$:Ce powder scintillators. *J. Lumin.* **2013**, *144*, 45–52. [CrossRef]
85. Evans, R.D. *The Atomic Nucleus*; McGraw-Hill: New York, NY, USA, 1955.
86. Seibert, J.; Boone, J. X-ray imaging physics for nuclear medicine technologists. Part 2: X-ray interactions and image formation. *J. Nucl. Med. Technol.* **2005**, *33*, 3–18. [PubMed]
87. Michail, C.; David, S.; Bakas, A.; Kalyvas, N.; Fountos, G.; Kandarakis, I.; Valais, I. Luminescence Efficiency of $(Lu,Gd)_2SiO_5$:Ce (LGSO:Ce) crystals under X-ray radiation. *Radiat. Meas.* **2015**, *80*, 1–9. [CrossRef]
88. Storm, E.; Israel, H. *Report LA-3753, Los Alamos Scientific Laboratory*; University of California: Oakland, CA, USA, 1967.
89. Yu, H.; Zhang, B.; Chen, X.; Qian, X.; Jiang, D.; Wu, Q.; Wang, J.; Xu, J.; Su, L. Color-tunable visible photoluminescence of Eu:CaF_2 single crystals: Variations of valence state and local lattice environment of Eu ions. *Opt. Express* **2019**, *27*, 523–532. [CrossRef]
90. Vartika, S.; Singh, V.; Joshi, C.; Moharil, S.; Muthal, P.; Dhopte, S. Modification of luminescence spectra of CaF_2:Eu^{2+}. *Luminescence* **2015**, *30*, 1101–1105.
91. Aiga, F.; Hiramatsu, R.; Ishida, K. *Ab initio* theoretical study of $4f \rightarrow 5d$ transitions in Eu^{2+}-doped CaF_2: (2) Augmented-basis-set-study. *J. Lumin.* **2016**, *169*, 601–605. [CrossRef]